A&A 513, A54 (2010)
DOI: 10.1051/0004-6361/200913137

Astronomy & Astrophysics

Stellar population and kinematics of NGC 404

A. Bouchard[1,2], P. Prugniel[2], M. Koleva[2,3,4], and M. Sharina[5,6]

[1] Department of Astronomy, University of Cape Town, Private Bag X3, Rondebosch 7701, Republic of South Africa
e-mail: bouchard@ast.uct.ac.za
[2] Université de Lyon, 69000 Lyon; Université Lyon 1, 69622 Villeurbanne; Centre de Recherche Astrophysique de Lyon; Observatoire de Lyon, 69561 St. Genis Laval; CNRS, UMR 5574, France
[3] Instituto de Astrofísica de Canarias, La Laguna, 38200 Tenerife, Spain
[4] Departamento de Astrofísica, Universidad de La Laguna, 38205 La Laguna, Tenerife, Spain
[5] Special Astrophysical Observatory of the Russian Academy of Sciences, Nizhnij Arkhyz, Karachaevo-Cherkessia, Russia
[6] Isaac Institute Chile, SAO Branch, Casilla 8-9, Correo 9, Santiago, Chile

Received 18 August 2009 / Accepted 8 January 2010

ABSTRACT

Context. NGC 404 is a nearly face-on, nearby low-luminosity lenticular galaxy. Probing its characteristics provides a wealth of information on the details of the possible evolution processes of dS0 galaxies, which may not be possible in other, more distant objects.
Aims. We study the internal kinematics and the spatial distribution of the star formation history in NGC 404.
Methods. We obtained long-slit spectroscopy at the OHP 1m93 telescope along the major and minor axes of NGC 404. The spectra had a resolution $R = 3600$ covering a wavelength range from 4600 to 5500 Å. The data were fitted against the Pegase. HR stellar population models to derive the internal stellar kinematics, ages, and metallicities simultaneously. All this was done while taking any instrumental contamination to the line-of-sight velocity distribution into account. First, the global properties of the galaxy were analysed by fitting a single model to the data and looking at the kinematic variations and SSP equivalent age and metallicities as a function of radius. Afterwards, the stellar populations were decomposed into 4 individually analysed components.
Results. NGC 404 clearly shows two radial velocity inversions along its major axis. The kinematically decoupled core rotates in the same direction as the neutral hydrogen shell that surrounds the galaxy. We resolved the star formation history in the core of the galaxy into 4 events: a very young (<150 Myr, and [Fe/H] = 0.4) component with constant ongoing star formation, a second young (430 Myr) component with [Fe/H] = 0.1, an intermediate population (1.7 Gyr) that has [Fe/H] = −0.05, and finally an old (12 Gyr) component with [Fe/H] = −1.26. The two young components fade very quickly with radius, leaving only the intermediate and old population at a radius of 25″ (370 pc) from the centre.
Conclusions. We conclude that NGC 404 had a spiral morphology about 1 Gyr ago and that one or many merger events has triggered a morphological transition. The interstellar medium in the galaxy has two components, the cold molecular gas is most probably a remnant from its past spiral incarnation and the outer neutral hydrogen layer that has probably been acquired in one of the latest mergers.

Key words. galaxies: abundances – galaxies: dwarf – galaxies: evolution – galaxies: stellar content – techniques: spectroscopic

1. Introduction

Although at the morphological intersection between spirals (S) and ellipticals (E), there may be more to lenticular galaxies (S0) than meets the eye. Indeed, while global properties of more massive S0 galaxies closely resemble those of giant Es, this is not the case for fainter objects (see van den Bergh 2009). Rather than being formed by the successive infall of galactic satellites, as seems to be the case for giant Es, the smaller S0s appear to essentially be remnants of gas depleted spirals (Bedregal et al. 2008). Several processes, including environmental effects (Moran et al. 2006) or galactic outflows caused by intense star formation (Davidge 2008), are possible causes of the ISM exhaustion, hence the transformation of spirals into S0s. These evolutionary scenarios may be particularly prominent in low-mass galaxies, as their weaker gravitational potential makes them more subject to gas depletion.

Recent discoveries of spiral arms, bars, and disks in several dEs and dS0s (Jerjen et al. 2000; Barazza et al. 2002; Graham et al. 2003; De Rijcke et al. 2003, 2004; Chilingarian et al. 2007; Lisker et al. 2007) have put a new twist on the debate on these objects' origin. It has been proposed that different formation mechanisms and progenitors were required to account for the diversity of the characteristics of the early-type dwarfs (nucleation, flattening, rotation, etc.) (van Zee et al. 2004; Lisker et al. 2008; Boselli et al. 2008). Dwarf irregulars (dIrrs) or BCDs may evolve into dEs and low luminosity S into dS0s (Aguerri et al. 2005).

At ~3.4 Mpc (Tonry et al. 2001; Karachentsev et al. 2002; Tikhonov et al. 2003), NGC 404 is the closest dS0 galaxy to the Local Group (see Table 1 for a summary of the targets' properties). It is also fairly isolated, the nearest neighbour being over 1 Mpc away (Karachentsev & Makarov 1999). This makes this nearly face-on galaxy (Barbon et al. 1982; del Río et al. 2004) a good test case for evolution scenarios, because one would expect minimal recent impact from any environmental effects (see Bouchard et al. 2009). This relative isolation coincides with active star formation (SF, Ho et al. 1993) and a dust lane with complex structure within 5″ from the centre (Barbon et al. 1982; Gallagher 1986; Wiklind & Henkel 1990;

Table 1. Properties of NGC 404.

Parameter	Value	Ref.
RA (J2000)	$01^h09^m27.0^s$	
Dec (J2000)	$+35°43'04''$	
Type	dS0	
$\epsilon = 1 - (b/a)$	0.07	1
D (Mpc)	3.05 ± 0.042	2
M_B	-16.26 ± 0.15	3
M_V	-17.63 ± 0.15	1
D_{25}	$3.5'$	4
	3.1 kpc	
r_e (*bulge*)	$61''$	5
	0.9 kpc	
M_{HI}	$1.5 \times 10^8\ M_\odot$	6
M_{HI}/L_B	$0.22\ M_\odot/L_\odot$	6

References. (1) Tikhonov et al. (2003); (2) Dalcanton et al. (2009); (3) Karachentsev et al. (2002); (4) de Vaucouleurs et al. (RC3, 1991); (5) Baggett et al. (1998); (6) del Río et al. (2004).

Ravindranath et al. 2001). del Río et al. (2004) find a ring of neutral hydrogen (H I) ($M_{HI} = 1.5 \times 10^8\ M_\odot$) surrounding the stellar disk, indicating that internal processes (most likely stellar feedback from intense SF within the molecular clouds) are evacuating the H I gas from the centre of the galaxy. NGC 404 has also a low-ionisation nuclear emission line region (LINER, Pogge et al. 2000).

By comparison, NGC 404 is only about 0.8 mag brighter than NGC 205 or the other dEs in nearby clusters presented in Koleva et al. (2009a). Should the remaining gas in this galaxy be expelled, stripped, or otherwise exhausted, the stellar population would fade and any remaining morphological "asymmetries" would vanish. This object would become very similar to any other early-type dwarf. In this paper we examine this possibility from the viewpoint of the stellar populations. Using long-slit optical spectroscopy along the major and minor axis (Fig. 1), we measured radial variations of the SF and metal enrichment histories within the central arc-minute of NGC 404.

This paper is organised as follows. Section 2 presents the data acquisition, reduction, and analysis strategy used in this paper. Section 3 presents age, metallicity, and the kinematical distribution profiles for this galaxy. In Sect. 4 we discuss a more in-depth approach to the SF history analysis. The overall discussion is found in Sect. 6 while the main conclusions are recalled in Sect. 7.

2. Observations

We used the OHP 1m93 telescope in November and December 2005 to obtain long-slit spectroscopic data of NGC 404 along 2 position angles (PA = 80° and PA = 170°, also referred to as the major and minor axes, see Fig. 1). The CARELEC spectrograph with the 1200 grating yielded a nominal dispersion of 33 Å/mm and a wavelength coverage from 4600 to 5500 Å. It had a central wavelength of λ_c = 5108 Å and $\lambda/\Delta\lambda = 3600$ (FWHM; instrumental velocity dispersion $\sigma_{ins} = 35\ km\ s^{-1}$)[1] and was equipped with a 0.325 mm slit. The EEV CCD (2048 × 1024 pixels) had a pixel of 13.5 μm or 0.45 Å × 0.54″. A total of 6 one-h frames were taken for the PA = 80° slit position and 7 one-h frame for PA = 170°.

[1] Measured on twilight spectra, see Fig. 3. The resolution relative to the Elodie library is $\sigma_{ins} = 33\ km\ s^{-1}$.

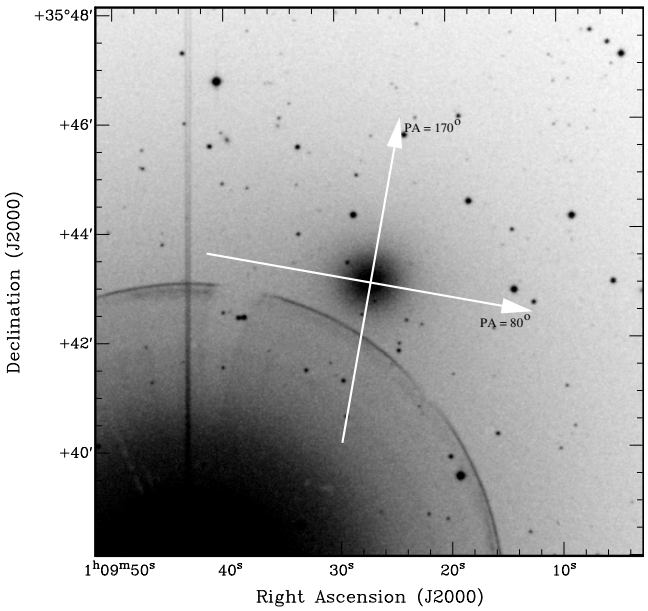

Fig. 1. DSS-2 image of NGC 404. The two observed PAs are shown in white, and the arrows indicate the direction of the spatial axis (see Fig. 5). The second magnitude foreground star β And contaminates the southeast corner of the image.

The galaxy has a very bright foreground star (β And, $m_V = 2$) approximately 5′ to the southeast. The star contaminates the spectra for radii greater than ~30 arcsec from the centre of the galaxy.

2.1. Data reduction

The data were reduced using the IRAF longslit spectroscopy package. After the bias subtraction, flat-fielding, wavelength calibration, and sky subtraction, the multiple exposures were co-added to produce one final image for each PA. No special effort was made to get rid of cosmic rays or other CCD defects because these can be handled later during the spectral fitting stage. There is a moderate number of such defects.

In the case of the radial profile analysis (see Sect. 3), the spectra were boxcar smoothed along the spatial axis to increase their signal-to-noise (S/N) ratio. In order to avoid smearing out the information in the central region, the smoothing kernel was taken to be 3 spatial pixels (~1.5″ or 22 pc at the distance of NGC 404) at the centre of the galaxy and increased linearly with radius to 29 pixels (~15″ or 220 pc) at angular offsets of ±60″. This resulted in $S/N \sim 50$ at $R = 0''$ and all spatial positions where $S/N \geq 1$ were analysed.

For the more detailed stellar population analysis presented in Sects. 3.2 and 4, the spectrum for the central region is an average of all spectra within 5″ (75 pc) from the centre of the galaxy (both PAs). The outer spectrum (at $R = 25''$ or 370 pc) is similarly a combination of all spectra between 15″ and 35″ from the centre of NGC 404.

2.2. Full spectrum fitting

The analysis was performed with *ULySS*[2] (Université de Lyon Spectroscopic analysis Software, Koleva et al. 2009b), a full spectrum-fitting software package. It fits an observed spectrum

[2] *ULySS* is available at http://ulyss.univ-lyon1.fr

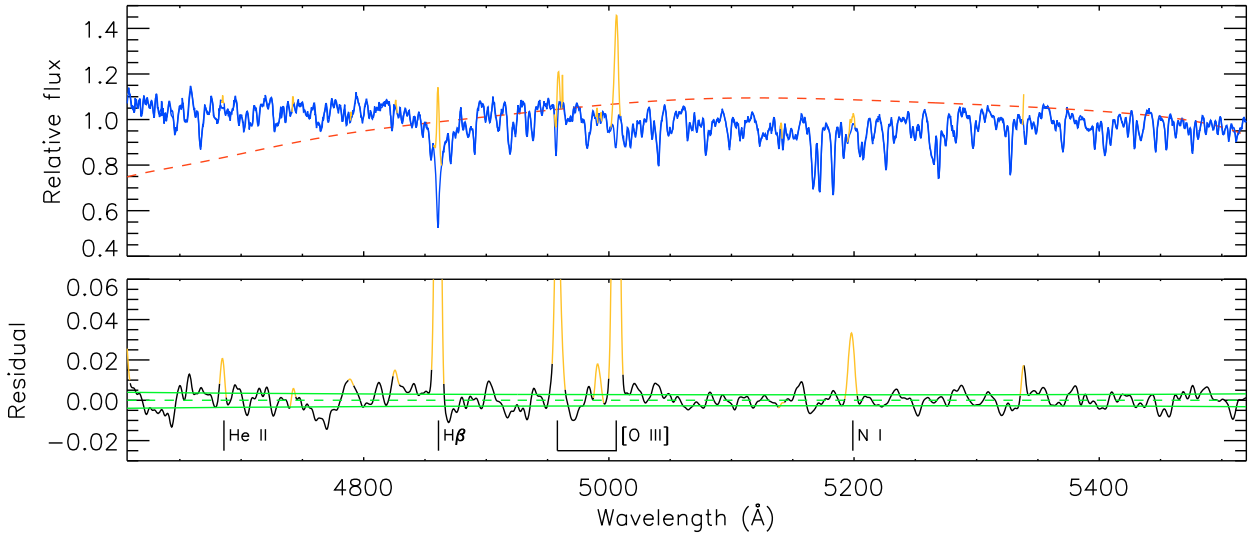

Fig. 2. Example fit as performed with *ULySS*. *The top panel* shows the data (black), the best-fitting model (blue), and the normalising polynomial (dashed red). The parts of the spectra that were ignored in the fitting procedure are plotted in orange. *The bottom panel* shows the fit residual smoothed to 100 km s^{-1} resolution; the green lines are the mean residual value (dashed) and $\pm 1\sigma$ residual deviation (solid). The best-fitting model here is a 4 component model as described in Sect. 4.

against a linear combination of nonlinear model components, convolved with a line-of-sight velocity distribution (LOSVD) and multiplied by a polynomial to absorb the effects of the flux calibration uncertainties and of the internal or Galactic extinction (see Sect. 2.3 for more details). The advantages of this program are (i) to use all the pixels (weighted by their inverse squared estimated errors) and (ii) to simultaneously minimise all the parameters leading to the optimal solution despite the degeneracies. This program is used to fit Single-age and Single-metallicity Population (SSP) models or composite models including the nebular emission lines and one or several SSPs.

The SSP spectra were generated using Pegase. HR (Le Borgne et al. 2004) and the ELODIE 3.1 stellar library (Prugniel & Soubiran 2001; Prugniel et al. 2007) that uses Salpeter (1955) initial mass function. A fit example is provided in Fig. 2 and the actual fitted model is a 4-population composite model and is described in Sect. 4.

The first step in the *ULySS* analysis is to evaluate the relative line spread function (LSF) between the models and the observed CARELEC spectra. This was done by comparing twilight sky spectra with a solar spectrum. The relative Gaussian broadening and velocity offset was determined with ULY_LSF in overlapping windows of 250 Å separated by 50 Å. The results are shown in Fig. 3. The velocity residuals, changing from −13 to −19 km s^{-1}, come from the uncertainty on the wavelength calibration (0.05 Å peak-to-peak). The decrease in the relative instrumental velocity dispersion, $\sigma_{\rm ins}$, from 35 km s^{-1} (blue) to 30 km s^{-1} (red) is a characteristic of the spectrograph and grating. This measured instrumental LSF is in turn used as an input parameter to *ULySS*, which *injects* it to the model before performing the minimisation (see Koleva et al. 2009b, for details).

2.3. Effects of dust extinction

In the case of a foreground dust screen (e.g. Galactic extinction), the absorption is a slowly varying function of wavelength and, in that respect, is exactly modelled by the low-resolution Legendre polynomial normalisation used in *ULySS* (provided that a single SSP is fitted). However, the dust has an

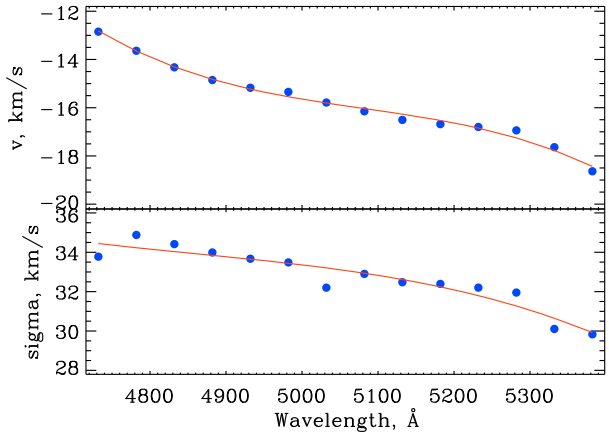

Fig. 3. Relative LSF ($v_{\rm rad}$, *top panel* and $\sigma_{\rm ins}$, *bottom panel*) between the observed spectra and the model as a function of wavelength. The blue dots represent the measured LSF, while the solid line is the smoothed version used as input for the rest of the analysis.

inhomogeneous distribution within the galaxy (cf., Wiklind & Henkel 1990) and the determination of the SFH (determined by fitting multiple SSPs) may be affected if the different generations of stars are absorbed differently.

Figure 4 compares the results of 2500 Monte-Carlo iterations where two different sets of SSP models (with or without dust) were used to determine the age of a composite stellar population. In this case, four simultaneous components (fully described in Sect. 4) were fitted to the core spectra of NGC 404. The value on the x-axis shows the age of the youngest SSP component found when neglecting dust effects compared with the age found when a free amount of dust absorption is added to each component. We adopted the Tojeiro et al. (2009) approach and took this effect into account by inserting a specific extinction on young stellar spectra (<1 Gyr).

It is clear from Fig. 4 that including absorption has a marginal effect: neglecting dust makes stars look younger and more metal rich (thereby more attractive), but the effect can be safely ignored because it is less than the accuracy of the

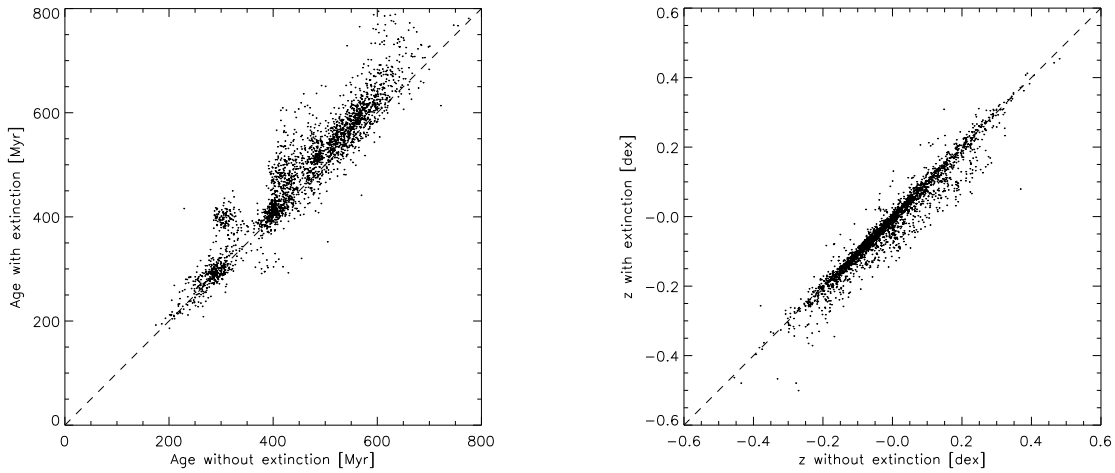

Fig. 4. Monte Carlo simulations of the effects of dust on the age (*left*) and z (*right*) measure for the youngest SSP component of a 4-component fit.

method (systematic shifts of the order of 50 Myr and 0.01 dex). The test recovers a very wide range in absorption measures with $A_B = 0.5 \pm 0.4$ mag, which implies that the method is globally insensitive to internal dust absorption, but it is doubtful that this value be reliable. In the remainder of this paper, we neglect any dust component in order to minimise the number of free parameters in the fits.

3. Radial profiles

Figure 5 presents luminosity, kinematical ($v_{\rm rad}$ and σ_v), and SSP equivalent age and metallicity profiles for the stellar population as a function of the radius for the two observed PAs. First the stellar population was adjusted with a single SSP using the automatic clipping of the outlier to reject the emission lines and the defects (option/CLEAN). The emission lines were then measured on the fit residuals. Since a preliminary analysis had shown that their kinematics were different, the [O III] doublet ($\lambda = 4958$ Å and 5006 Å) and the Hβ line ($\lambda = 4861$ Å) were fitted separately, i.e., independently determining the kinematics of both systems.

3.1. Stellar and ISM kinematics

The $v_{\rm rad}$ profile along the major axis (PA = 80°) shows a complicated structure with what appears to be a double inversion of the velocity gradient. The core, within ±1″ from the centre, is in counter-rotation with a 2.2 km s^{-1} amplitude. The surrounding region displays a linear velocity gradient until ±20″ (±295 pc at the distance of NGC 404) from the center where the apparent rotation reaches ~23 km s^{-1}. From this radius outward, the rotation velocity decreases to inverse its direction at ~35″ (520 pc). At very large radii, the velocity profile is consistent with the results of del Río et al. (2004), who measured an H I rotational (i.e., deprojected) velocity to be ~200 km s^{-1}. Otherwise, no rotation is seen along the minor axis.

The central velocity dispersion, i.e., the average σ_v value in the inner 5″ (75 pc) for both PAs, is $\sigma_v^c = 30 \pm 2$ km s^{-1}. This is substantially lower than previous measurements. Barth et al. (2002) found $\sigma_v = 40 \pm 3$ km s^{-1} from the near-infrared [Ca II] triplet. Our new value is, however, comparable to the central velocity dispersion of the slightly fainter NGC 205 ($\sigma_v^c = 20 \pm 1$ km s^{-1}, Simien & Prugniel 2002). With $L_B = 10^{8.7}\ L_\odot$ (Karachentsev et al. 2002), it is also consistent with the Faber & Jackson (1976) relation for dwarf galaxies (see de Rijcke et al. 2005).

Spectra near the centre of NGC 404 clearly show Hβ ($\lambda = 4861$ Å) and [O III] ($\lambda = 4958$ and 5006 Å) emission-lines originating in the star-forming regions in the ISM and the active nucleus. Figure 5 also shows the flux, radial velocity, and velocity dispersion for Hβ and [O III]. The intensity profiles of Hβ along both axes are symmetrical, unlike those of the [O III] lines which present a secondary peak around 10″ (150 pc) to the East of the centre, along the major axis. This off-centred peak corresponds the position of a giant molecular cloud that was detected with CO observations (Wiklind & Henkel 1990).

Globally, the ionised gas distribution is flattened more than the stellar population: the full widths at 20% of maximum (FW20) for Hβ are 8.8″ and 6.8″ for the major and minor axes, respectively and 15.0 and 7.5″ for [O III] (excluding the secondary peak). This indicates ellipticities of $\epsilon_{\rm H\beta} = 0.22$ and $\epsilon_{\rm [O\,III]} = 0.5$, compared with $\epsilon_{\rm stars} = 0.12$. Tikhonov et al. (2003) find a stellar ellipticity of 0.07.

The ISM and stellar velocity profiles agree well within the measured range, and the Hβ width is comparable to the stellar velocity dispersion. The [O III] emission line, however, has a significantly higher dispersion than Hβ in the central 10″ along both axes, and the central velocity dispersion reaches 70 km s^{-1}.

3.2. Stellar populations

The SSP-equivalent age and [Fe/H] profiles (Fig. 5) show similar behaviour for both axes. In the star-forming region, i.e., within a radius of 20″(295 pc), the SSP-equivalent age increases from the central value of 1.3 Gyr to 1.7 Gyr, while the metallicity remains relatively constant at −0.2. Outside of this region and to the edge of the measurements at about 1 $R_{\rm e}$, the age rises to 10 Gyr and the metallicity drops down to −0.6. These gradients are qualitatively and quantitatively similar to those observed in other dEs and dS0s (Koleva et al. 2009a; Chilingarian 2009).

Figure 6 shows a χ^2 map (made with the program ULY_CHIMAP in the age vs. metallicity plane) for a spectrum extracted within a radius of 5″ (75 pc) from the centre. The map reveals a local minimum (near 4 Gyr and −0.5 dex) that requires to perform a global minimisation, achieved by using a grid of initial guesses. A series of 2000 Monte-Carlo simulations (Fig. 6), each time adding a random noise equivalent to the observation noise estimated from the characteristics of the detector,

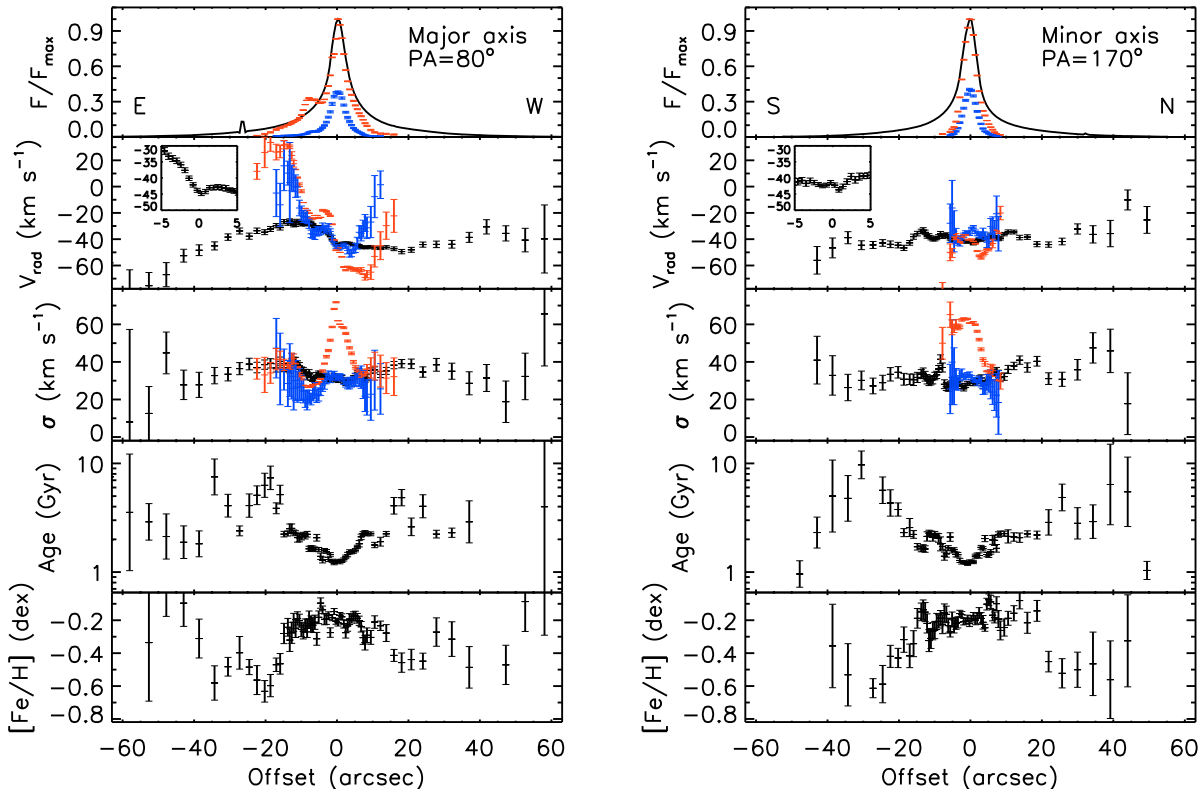

Fig. 5. Radial profiles for normalised flux (*top panel*), $v_{\rm rad}$ (2nd panel), σ_v (*middle panel*), Age (4th panel), and [Fe/H] (*bottom panel*) for the two observed PA of NGC 404 (major axes, PA = 80° on *the left* and minor axis, PA = 170° on *the right*). Overplotted on *the top three panels* are the profiles derived from the Hβ (blue) and [O III] (red) emission lines. The flux values for [O III] are the sum of the λ = 4958 and 5006 Å lines and are normalized to the central total flux with Hβ flux plotted on the same scale. The insets on the second panels show a zoom on the central stellar velocity profiles.

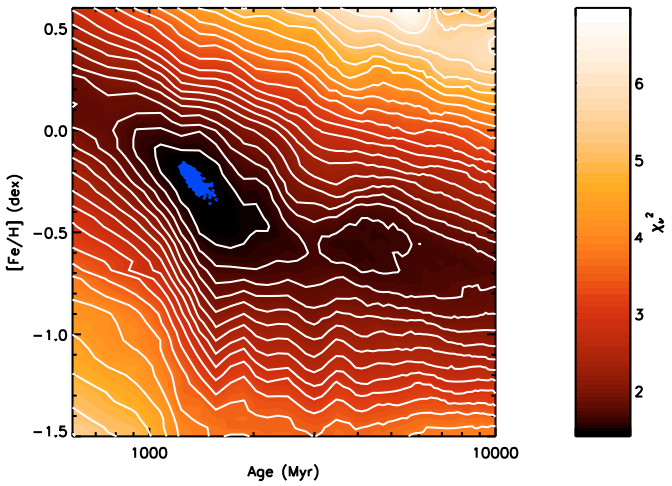

Fig. 6. χ^2_ν distribution map for a single stellar population model fit of NGC 404 as a function of age and [Fe/H]. Lines of constant χ^2_ν are overplotted (white). The blue dots represent the result of Monte Carlo simulation.

was used to properly estimate the precision of the measurements. The resulting SSP-equivalent parameters are reported in Table 2 (age = 1319 ± 41 Myr and [Fe/H] = −0.225 ± 0.016 dex).

4. Star formation history

As the presence of extended nebular emission lines in the spectra is evidence of ongoing SF in the central region of NGC 404, it is clear that an SSP is not a good representation of the real stellar population. The radial increase in the SSP-equivalent age (Fig. 5) may in fact reflect the decreasing fractional contribution of a young and centrally concentrated SF burst with respect to an older, more uniform stellar population. We therefore reconstructed the star formation history (SFH) of NGC 404 following the approach adopted in Koleva et al. (2009a), i.e., by decomposing the observed spectra in a sum of several components. We adopted a 4-component model consisting of three SSPs representing various stellar populations in the galaxy, plus one young population with constant, ongoing SF rate (CST). The latter component was also produced using Pegase. HR with the Elodie 3.1 library and Salpeter IMF.

Table 2. Star formation history.

SFH type	f_L (%)	f_M (%)	Age (Myr)	[Fe/H] (dex)
		Core (SSP-equivalent)		
SSP	...	...	1319 ± 41	−0.225 ± 0.016
		Core (4 components)		
CST	4.1 ± 0.5	0.20 ± 0.03	150	0.4 ± 0.3
SSP	20 ± 1	5.6 ± 0.3	430 ± 100	0.1 ± 0.1
SSP	62 ± 1	58 ± 1	1700 ± 160	−0.05 ± 0.05
SSP	14 ± 1	36 ± 2	12 000	−1.26
		R=25″		
SSP	47 ± 2	37 ± 1	2600 ± 400	0.16 ± 0.15
SSP	53 ± 2	63 ± 2	12 000	−1.26 ± 0.22

The age limits between each component were essentially chosen on a trial and error basis. The method consists in choosing an initial set of populations with the age limits distributed evenly on a logarithmic axis. If any of the fitted populations returned a result that was equal to its boundary limit, then that "population box" was either merged with the adjacent one or the limits modified. In some cases, mainly when a population showed incoherent behaviour after a box merger or has non-reproducible results under a global minimisation attempt (i.e. providing multiple initial guesses inside the set limits), then an adjacent box was split in two to increase resolution and the process carried on. The solution was considered valid when none of the population's parameters reached any of the set limits and was robust with a Monte Carlo approach.

In the end, the limits were set as follows:

- the old SSP has a fixed age = 12 Gyr;
- the intermediate age SSP has 800 < age < 6000 Myr;
- the youngest SSP has age < 800 Myr;
- the CST population began its SF 150 Myr ago.

No further limits were imposed on metallicity.

This 4-component analysis was applied at two different locations: first at the edge of the star-forming region ($R = 25''$ or 370 pc) and then in the core of NGC 404 ($R = 0''$, see Sect. 2.1 for more details about these spectra). The results are summarised in Table 2: the first column shows the type of stellar population that was fitted, the second and third columns are the relative stellar luminosity and stellar mass fraction for each of the component, Col. 4 shows the measured age of each population, and finally the last column contains their metallicity. The results are more significant than the single SSP fit, and the χ^2_ν is reduced from 1.4 (single SSP) to 1.001 (4 component).

Old, low metallicity ([Fe/H] = −1.26 dex) stars contribute to 63% of the stellar mass just outside of the SF region, taking stellar mass loss due to normal stellar evolution into account. There is also a high fraction (37%) of intermediate age (2.6 Gyr) and high metallicity (0.16 dex) stars. As expected, we found no traces of any young population (SSP and CST), no emission lines were seen in the spectra at that location. Our results for the old population are in good agreement with those from HST stellar photometry ([Fe/H] = −1.11 dex, Tikhonov et al. 2003).

Similar analysis was done in the core ($R = 0''$). Although old stellar populations of early type dwarfs often exhibit radial metallicity gradients (Harbeck et al. 2001; Koleva et al. 2009a), we kept the metallicity fixed at [Fe/H] = −1.26 (the value found at $R = 25''$). This was done partly to minimise the number of free parameters in the fit and because, in the presence of a strong young population (luminosity-wise), there is a limit to the amount of information on the older stars that can be extracted from a given spectrum.

As expected from Fig. 5, the mass fraction contributed by old stars decreased to 36%, giving way to a larger (58%) and somewhat younger (1.7 Gyr) intermediate population with solar metallicity ([Fe/H] = −0.05). We also see a non-negligible (6%) young stellar population (430 Myr) and traces of ongoing SF within the last 150 Myr (0.2% in mass).

To verify the reproducibility and accuracy of our results in the centre of NGC 404, we used two additional spectra from the Fast Spectrograph for the Tillinghast Telescope (FAST, Fabricant et al. 1998) archive[3]. The data are 120 s exposures on a 1.5 m telescope with 1.47 Å pixel^{-1}, covering 3700 to 7500 Å.

[3] http://tdc-www.harvard.edu/instruments/fast/

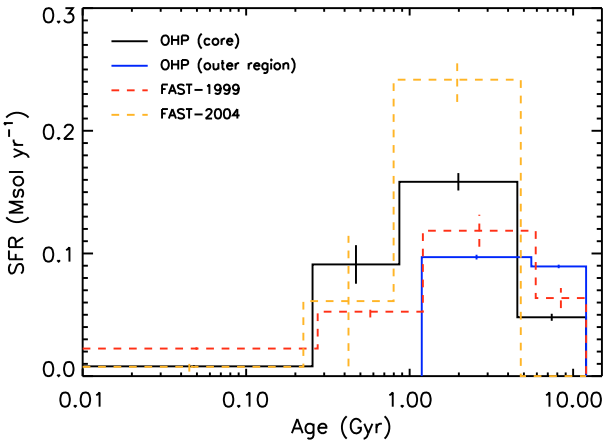

Fig. 7. SFR as a function of lookback time for an assumed total stellar mass of 1×10^9 $M_\odot$. The black line shows the SFR from the centre of NGC 404, the blue shows the outer region. For comparison, we have also plotted results of two FAST spectra, the 1999 data in red and 2004 in gold.

The spectra were obtained on taken on October 12, 1999 and July 19, 2004.

Figure 7 presents the results of a similar, 4-component model analysis, on all four spectra. It shows the required SFR as a function of age (lookback time) to produce the measured stellar population ages and relative importance. The age limits for the bins are chosen to be the halfway point between the measured ages of the components, also imposing a maximum age of 12 Gyr. Although they have more or less comparable overall masses (Table 2), the SFR associated with the old stellar population is lower but distributed over a longer period than for the intermediate population.

The results for the 3 core spectra are consistent on a qualitative level: all 3 have some level of ongoing SF and similar distribution for the three SSP components. The only exception is for the FAST-2004 spectra that shows no evidence of the old stellar population but a stronger intermediate-age one. The outer region seems to have had a more uniform SFH, indicating that the SF burst is concentrated in the inner few arc-seconds.

We also traced the stellar light and mass distribution for each of the 4 components as a function of radius as shown in Fig. 8. To accomplish this, the age and metallicity of each component were fixed to the values found in the core of NGC 404 (Table 2), leaving only the relative fraction to vary with radius. These mass and light fractions resulting from the various fits were then converted to an absolute distribution by scaling our results to the values measured by Tikhonov et al. (2003) and Dalcanton et al. (2009), i.e., $\mu_{V,0} = 16.6$, $D = 3.05$ Mpc, respectively, and the stellar mass-to-light ratio derived from the fitted models (on average $M/L_V = 0.7$).

We can indeed see from Fig. 8 that the two young components are both centrally concentrated and have similar distribution, since they are found within 10″ (150 pc) from the core of NGC 404. This corresponds to the size of the molecular cloud found by Wiklind & Henkel (1990). The ages of these two components and their different metallicities lead to the conclusion that the period over which this galaxy sustained more or less constant SFR is probably much longer than what the 150 Myr CST burst suggests. The galaxy core has seen substantial chemical enrichment throughout the last Gyr.

The two older stellar populations have radially varying importance and the stellar light from the old population becomes

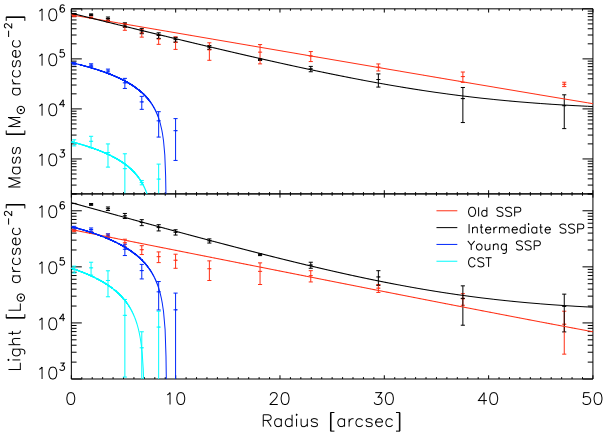

Fig. 8. Stellar mass (*top*) and stellar light (*bottom*) distribution of each population as a function of radius. The old stellar population is in red, the intermediary in black, the young in dark blue and the very young population with constant SFR is in cyan. The lines show the results of exponential fits through the data points.

dominant at radii larger than 30″. Tikhonov et al. (2003) reached a similar conclusion from their optical photometry studies. In that respect, NGC 404 is similar to the elliptical galaxy NGC 205 where the central cluster, HubbleV, is younger and more metal-rich than the surrounding fields. There are also age and metallicity gradients for the field stellar populations of this galaxy (see Sharina et al. 2006, for more details).

5. Discussion

NGC 404 has a very peculiar kinematical structure with two velocity gradient inversions (Fig. 5), and the innermost region ($R < 3''$ or 45 pc) of the galaxy rotates in the same direction has the H I gas (del Río et al. 2004). This inner core is also the region where the youngest stars are found (Fig. 8). Although *ULySS* does not allow us to independently track the kinematics of each individual model component, it seems that this counter-rotation is a feature affecting only the newly-created stars. This suggests that the ongoing SF may have been triggered by the relatively recent ($\lesssim$500 Myr) accretion of a nearby gas-rich, low-mass companion. Our results are in perfect agreement with those of del Río et al. (2004), who argued that such an encounter must have happened approximately 0.5×10^9 Gyr ago in the case of a catastrophic merger. This is the required timescale to allow H I gas to settle in the plane for the inner ring but not the outer one. This sort of encounter would result in SF at the centre of the galaxy and exhibit the observed distinctive kinematical features.

Considering the scenario where dS0s are formed by the harassment and gas removal in late type spirals (Aguerri et al. 2005), this places NGC 404 in the awkward position of having *acquired* gas rather than having it removed. However, since the galaxy obviously had multiple past encounters, it is not surprising to see a morphological transition. The overall angular momentum of the old stellar population indicates that this galaxy was in rotation prior to its last merger. Furthermore, there is a significant, broadly distributed, intermediate age stellar population (1.7 Gyr), which could have been produced during a past, more or less extended period of active star formation (see Fig. 7). We conclude that this system has been a spiral 1 Gyr ago, and the cold molecular gas found in the centre of NGC 404 (Wiklind & Henkel 1990) is probably a relic from those earlier times (Temi et al. 2009).

Sharina et al. (in prep.) find GCs in NGC 404 and measured age and metallicity for one of them, using medium-resolution spectra obtained with the SCORPIO spectrograph at the 6 m telescope. It appears to be old (10 Gyr) and metal-poor [Z/H] ~ -1.7 dex. Its properties are similar to those of the old stellar population of NGC 404 and it is probably part of the entire system, having been formed during the initial SF epoch.

Maoz et al. (1998) classified NGC 404 has a UV-bright low ionisation nuclear emission line region (LINER) galaxy, and the emission lines seen in Fig. 2 (namely Hβ, [O III], He II and N I) are indeed typical of the high ionisation range seen in narrow line active galaxy nuclei (AGN). On one hand, the apparent kinematic decoupling between the [O III] and Hβ line emission (Fig. 5) may be explained by this as the [O III] may have components coming from both the nebular component of the galaxy and its AGN, so the width of the two lines would naturally decorrelate. On the other hand, since oxygen is mainly produced by very massive stars, the coincidence of the high [O III] activity with the GMC may be a sign of a massive star burst (maybe the formation of a new stellar cluster), hence a region of intensive stellar winds and greater gas turbulence. Interestingly, this region is near but somewhat offset from the centre of NGC 404, reminiscent of circumnuclear rings often found in S0 galaxies (e.g., Sil'chenko & Afanasiev 2002)

The SF in NGC 404 is clearly confined within 150 pc (10″) of its centre (Fig. 8). Overall, it remains of low level: nowhere does the newly formed stars (<1 Gyr) dominate the mass budget of the galaxy. (It is less than 6% in the centre.) Unless future catastrophic events shape the evolution of this object, NGC 404 should continue on this "slow" evolutionary track, and there is no reason to think that any significant SF would occur at large radii. The mechanisms that lead this object from its past spiral morphology to its current dS0 state should continue their action until SF definitely stops in this object, either because of fuel exhaustion or other gas removal mechanisms.

6. Conclusion

We obtained spectroscopic observation along two position angles for the nearby dS0 galaxy NGC 404. The spectra were analysed using the *ULySS* full spectral-fitting package to find SSP equivalent ages, metallicities, and kinematics for the different stellar populations.

Kinematically, the galaxy shows hints of a double radial velocity inversion, a sign of multiple past encounters. This probably triggered the evolution process leading the galaxy from a previous spiral morphology (1 Gyr ago) to the current dS0 one. One of the latest merger event (with an H I rich companion) would have triggered the most recent SF episode which lasted for about 450 Myr.

We resolved the SF history of NGC 404 into 4 events whose relative importance varies with radius. The youngest component has high metallicity ([Fe/H] = 0.4 ± 0.3) and ongoing SF that has lasted for 150 Myr. Another young component of age 430 Myr has near solar metallicity ([Fe/H] = 0.1 ± 0.1). Both these component make a negligible contribution to the spectra of NGC 404 at a radius greater than 10″ or 150 pc. The dominating stellar population is of intermediate age and near solar metallicity. Its SSP equivalent parameters vary from 1.7 Gyr and [Fe/H] = −0.05 ± 0.05 in the centre to 2.6 Gyr and [Fe/H] = 0.16 ± 0.15 at 370 pc from the centre (a radius of 25″). Finally, the last stellar population has an age of 12 Gyr and [Fe/H] = −1.26. The decomposition of the history in a succession of bursts is an input characteristic of our model, and the

time resolution is limited by the quality of the models and of the observations and by the intrinsic degeneracies of the problem. The metallicity history was not constrained and reveals a realistic progressive enrichment. Considering that the impact of internal dust absorption was shown to have a negligible effect on the recovered SF history, it was therefore ignored to lower the number of free parameters in the fits.

The kinematical and chemical history of NGC 404 is consistent with it having evolved from a spiral morphology to a dS0 state. Future evolution will most probably continue this ongoing transition and, should we revisit this system in a few Gyr, we would most likely find a dE.

Acknowledgements. We are grateful to François Simien who contributed to the early phases of this project, to Dmitry Makarov for his help during data reduction, and to the anonymous referee for the useful comments. A.B. acknowledges financial support from the South African Square Kilometre Array Project. M.K. acknowledges support by the Programa Nacional de Astronomía y Astrofísica of the Spanish Ministry of Science and Innovation under grant *AYA2007-67752-C03-01*. M.S. is partially supported by Russian Foundation for Basic Research grant *08-02-00627*. We thank the Programme National Galaxies, from the French CNRS, for granting the observation time, and the staff from the Observatoire de Haute-Provence for their support during the observations.

References

Aguerri, J. A. L., Iglesias-Páramo, J., Vílchez, J. M., Muñoz-Tuñón, C., & Sánchez-Janssen, R. 2005, AJ, 130, 475
Baggett, W. E., Baggett, S. M., & Anderson, K. S. J. 1998, AJ, 116, 1626
Barazza, F. D., Binggeli, B., & Jerjen, H. 2002, A&A, 391, 823
Barbon, R., Capaccioli, M., & Rampazzo, R. 1982, A&A, 115, 388
Barth, A. J., Ho, L. C., & Sargent, W. L. W. 2002, AJ, 124, 2607
Bedregal, A. G., Aragón-Salamanca, A., Merrifield, M. R., & Cardiel, N. 2008, MNRAS, 387, 660
Boselli, A., Boissier, S., Cortese, L., & Gavazzi, G. 2008, ApJ, 674, 742
Bouchard, A., Da Costa, G. S., & Jerjen, H. 2009, AJ, 137, 3038
Chilingarian, I. V. 2009, MNRAS, 394, 1229
Chilingarian, I. V., Prugniel, P., Sil'Chenko, O. K., & Afanasiev, V. L. 2007, MNRAS, 376, 1033
Dalcanton, J. J., Williams, B. F., Seth, A. C., et al. 2009, ApJS, 183, 67
Davidge, T. J. 2008, AJ, 135, 1636
De Rijcke, S., Dejonghe, H., Zeilinger, W. W., & Hau, G. K. T. 2003, A&A, 400, 119
De Rijcke, S., Dejonghe, H., Zeilinger, W. W., & Hau, G. K. T. 2004, A&A, 426, 53
de Rijcke, S., Michielsen, D., Dejonghe, H., Zeilinger, W. W., & Hau, G. K. T. 2005, A&A, 438, 491
de Vaucouleurs, G., de Vaucouleurs, A., Corwin, Jr., H. G., et al. 1991, Third Reference Catalogue of Bright Galaxies
del Río, M. S., Brinks, E., & Cepa, J. 2004, AJ, 128, 89
Faber, S. M., & Jackson, R. E. 1976, ApJ, 204, 668
Fabricant, D., Cheimets, P., Caldwell, N., & Geary, J. 1998, PASP, 110, 79
Gallagher, III, J. S. 1986, PASP, 98, 81
Graham, A. W., Jerjen, H., & Guzmán, R. 2003, AJ, 126, 1787
Harbeck, D., Grebel, E. K., Holtzman, J., et al. 2001, AJ, 122, 3092
Ho, L. C., Filippenko, A. V., & Sargent, W. L. W. 1993, ApJ, 417, 63
Jerjen, H., Kalnajs, A., & Binggeli, B. 2000, A&A, 358, 845
Karachentsev, I. D., & Makarov, D. I. 1999, in Galaxy Interactions at Low and High Redshift, ed. J. E. Barnes, & D. B. Sanders, IAU Symp., 186, 109
Karachentsev, I. D., Sharina, M. E., Makarov, D. I., et al. 2002, A&A, 389, 812
Koleva, M., de Rijcke, S., Prugniel, P., Zeilinger, W. W., & Michielsen, D. 2009a, MNRAS, 396, 2133
Koleva, M., Prugniel, P., Bouchard, A., & Wu, Y. 2009b, A&A, 501, 1269
Le Borgne, D., Rocca-Volmerange, B., Prugniel, P., et al. 2004, A&A, 425, 881
Lisker, T., Grebel, E. K., Binggeli, B., & Glatt, K. 2007, ApJ, 660, 1186
Lisker, T., Grebel, E. K., & Binggeli, B. 2008, AJ, 135, 380
Maoz, D., Koratkar, A., Shields, J. C., et al. 1998, AJ, 116, 55
Moran, S. M., Ellis, R. S., Treu, T., et al. 2006, ApJ, 641, L97
Pogge, R. W., Maoz, D., Ho, L. C., & Eracleous, M. 2000, ApJ, 532, 323
Prugniel, P., & Soubiran, C. 2001, A&A, 369, 1048
Prugniel, P., Soubiran, C., Koleva, M., & Le Borgne, D. 2007 [arXiv:astro-ph/0703658]
Ravindranath, S., Ho, L. C., Peng, C. Y., Filippenko, A. V., & Sargent, W. L. W. 2001, AJ, 122, 653
Salpeter, E. E. 1955, ApJ, 121, 161
Sharina, M. E., Afanasiev, V. L., & Puzia, T. H. 2006, MNRAS, 372, 1259
Sil'chenko, O. K., & Afanasiev, V. L. 2002, A&A, 385, 1
Simien, F., & Prugniel, P. 2002, A&A, 384, 371
Temi, P., Brighenti, F., & Mathews, W. G. 2009, ApJ, 695, 1
Tikhonov, N. A., Galazutdinova, O. A., & Aparicio, A. 2003, A&A, 401, 863
Tojeiro, R., Wilkins, S., Heavens, A. F., Panter, B., & Jimenez, R. 2009, ApJS, 185, 1
Tonry, J. L., Dressler, A., Blakeslee, J. P., et al. 2001, ApJ, 546, 681
van den Bergh, S. 2009, ApJ, 694, L120
van Zee, L., Barton, E. J., & Skillman, E. D. 2004, AJ, 128, 2797
Wiklind, T., & Henkel, C. 1990, A&A, 227, 394